Journal of Solid State Chemistry 185 (2012) 31–36

Contents lists available at SciVerse ScienceDirect

Journal of Solid State Chemistry

journal homepage: www.elsevier.com/locate/jssc

Microstructure, magnetic properties and exchange–coupling interactions for one-dimensional hard/soft ferrite nanofibers

Fuzhan Song, Xiangqian Shen*, Mingquan Liu, Jun Xiang

School of Materials Science and Engineering, Jiangsu University, Zhenjiang 212013, PR China

ARTICLE INFO

Article history:
Received 8 June 2011
Received in revised form
5 September 2011
Accepted 9 October 2011
Available online 15 October 2011

Keywords:
Ferrite
Nanofiber
Composite
Magnetic property
Exchange–coupling

ABSTRACT

$SrFe_{12}O_{19}$ (SFO)/$Ni_{0.5}Zn_{0.5}Fe_2O_4$ (NZFO) composite ferrite nanofibers with diameters about 120 nm have been prepared by the electrospinning and calcination process. The SFO/NZFO composite ferrites are formed after calcined at 700 °C for 2 h and the composite nanofibers with various mass ratios obtained at 900 °C are fabricated from NZFO grains about 16–40 nm and SFO grains of 19–45 nm with a uniform phase distribution. With the SFO ferrite content increasing, the coercivity (H_c) and remanence (M_r) for the composite ferrite nanofibers initially increase, reaching maximum values of 379.8 kA/m (297 K) and 242.2 kA/m (77 K), 39.1 Am^2/kg (297 K) and 53.5 Am^2/kg (77 K), respectively, at a mass ratio (SFO:NZFO) of 4, and then show a reduction tendency with a further increase of the mass ratio. This enhancement in magnetic properties is attributed to the competition of the exchange–coupling interaction and the dipolar interaction in the composite nanofibers.

1. Introduction

Nanocomposite magnetic materials have attracted numerous studies since the composite of different magnets in a nanoscale can drastically improve the overall magnetic properties based on the exchange spring mechanism. They can be widely used in magnetic recording media, magnetic fluids, microwave devices, permanent magnets and biomedicines [1–5]. For example, Doyle et al. [6] recently reported the rapid separation of intact λ–DNA in only 10–15 min using self-assembled nanocomposite magnetic arrays.

According to the exchange spring concept, a composite magnet combining the high coercivity of the hard phase and the high saturation magnetization of the soft phase is recognized as an exchange spring magnet [7,8]. The magnetic properties of the nanocomposite magnets are highly sensitive to grain size, microstructure, distribution of the soft and hard phases and impurity [9]. In addition, the exchange length is a key factor for the exchange–coupling interaction in nanocomposite magnets. The exchange length of the crystal could cover some part of the neighboring grains, which improves the exchange–coupling interaction. Recently, Suzuki and Cadogan [10] studied the exchange length of $Fe_{91}Zr_7B_2$ nanocrystallites at different temperatures and discussed the effect of exchange length on the exchange–coupling interaction. However, for nanocomposite powders, as the nanoparticles have a strong tendency to aggregate [11], the aggregated particles are usually beyond the exchange length and the powders so that could not be sufficiently exchange–coupled.

One-dimensional (1D) nanostructured materials including nanotubes, nanowires, nanofibers and nanobelts have attracted much attention due to their novel properties in referring to bulk or particle counterparts and their potential applications for ultrahigh-density data storages, magnetic sensors, micro/nano electromagnetic devices, spin electric devices, catalytic and magnetic composites [12–15]. In addition, 1D nanocomposite materials could restrain the aggregation of particles due to shape characteristics and improve the exchange–coupled interaction effectively. Among various 1D nanoshapes, nanofibers have a considerable importance technologically due to a high aspect ratio and anisotropic characteristic.

Compared to the widely used metallic Nd–Fe–B and Sm–Co systems [16,17], the nanocomposite ferrites consisting of the hard M-type ferrite and the soft spinel ferrite are promising advanced permanent magnetic materials due to a low cost and an excellent corrosion resistance [18–21]. Recently, nanocomposite powders of the soft (Fe_3O_4)–hard ($BaCa_2Fe_{16}O_{27}$) ferrites, soft ($Ni_{0.8}Zn_{0.2}Fe_2O_4$)–hard ($BaFe_{12}O_{19}$) ferrites were reported and the exchange spring phenomena in these hard–soft ferrite nanocomposites were observed [8,22]. Based on our previous work for the SFO/NZFO ferrite hollow microfibers [23], this work reported the fabrication of SFO/NZFO composite ferrite nanofibers with different mass ratios utilizing the sol–gel assisted electrospinning and characterization of the chemical composition, microstructure and magnetic properties measured at 77 K and 297 K for these SFO/NZFO composite ferrite nanofibers.

* Corresponding author. Fax: +86 511 88791964.
E-mail address: shenxq@ujs.edu.cn (X. Shen).

0022-4596/$ - see front matter © 2011 Elsevier Inc. All rights reserved.
doi:10.1016/j.jssc.2011.10.009

2. Experimental

The preparation of SFO/NZFO composite ferrite nanofibers with different mass ratios (SFO:NZFO = 1:9, 2:8, 3:7, 4:6, 5:5, 6:4, 7:3, 8:2 and 9:1) consisted of solution preparation, electrospinning and calcination. In the solution preparation, the required amount of polyvinylpyrrolidone (PVP, molecular weight 1,300,000, Aldrich) was dissolved in ethanol to form a PVP/ethanol solution. Then according to the different mass ratios, the required strontium nitrate ($Sr(NO_3)_2$, AR), nickel acetate ($C_4H_6NiO_4 \cdot 4H_2O$, AR), zinc acetate ($C_4H_6O_4Zn \cdot 2H_2O$, AR), ferric nitrate ($Fe(NO_3)_3 \cdot 9H_2O$, AR), and distill water were added into the PVP/ethanol solution and magnetically stirred about 24 h at room temperature. The viscous solution was loaded into a plastic syringe with a stainless steel needle. The needle used as the positive electrode was connected to a high-voltage supply and the solution was fed at a rate of 0.5 mL/h using a syringe pump during the electrospinning process. A piece of aluminum foil used as the ground collector was placed in front of the needle tip to collect the composite nanofibers. The distance between syringe needle tip and collector was 15 cm and the applied voltage was 15 kV. The as-spun SFO/NZFO composite precursor nanofibers collected were dried and calcined at different temperatures for 2 h in ambient atmosphere to obtain SFO/NZFO composite ferrite nanofibers with different mass ratios.

The X-ray diffraction (XRD) patterns were collected on a Rigaku D/Mmax2500PC diffractometer with Cu-$K\alpha$ radiation. Field emission scanning electron microscopy (FE-SEM, JSM-7001F) equipped with an Oxford INCA energy-dispersive X-ray (EDX) spectrometer and transmission electron microscopy (TEM, JEM-2100) were employed to analyze the morphology and chemical composition of the samples. The magnetic properties of the resultant nanofibers were investigated using a vibrating sample magnetometer (VSM, HH-15) with a maximum applied field of 1194 kA/m (15 kOe).

3. Results and discussion

Fig. 1 shows SEM images (a–c), XRD patterns (d) and EDX spectrum (e) of SFO/NZFO composite ferrite nanofibers with mass ratio of 8:2 calcined at different temperatures for 2 h. From Fig. 1(a), it shows that these nanofibers with high aspect ratio possess a uniform diameter ranging from 100 to 150 nm. After calcined at 750 °C for 2 h (Fig. Fig. 1(b)), some hexagonal plate-like particles are observed, which are embedded in the nanocomposite ferrite microfiber. With the calcination temperature increased to 900 °C, the particle growth takes place and more and more hexagonal plate-like particles form on the microfiber's surface. It is interesting to note that smaller NZFO ferrite particles tend to adsorb on planes of larger hexagonal plate-like SFO particles in the nanocomposite ferrite nanofibers (as shown in Fig. 1c)). This phenomenon can be attributed to the fact the NZFO ferrite has a spinel structure, which is similar to **S** blocks in the strontium ferrite [22]. The NZFO structure therefore is compatible with the strontium ferrite and a strong exchange–couple can be anticipated between these hard (SFO) and soft (NZFO) ferrites in the composite nanofibers.

Fig. 1(d) shows that after calcined at 700 °C, the XRD diffractions are indexed to the coexistence of the magnetoplumbite SFO phase (JCPDS 33-1340) and spinel NZFO phase (JCPDS 53-0278). With the calcination temperature up to 900 °C, the XRD diffractions corresponding to SFO and NZFO ferrites do not alter, except that the reflection peaks become narrower and higher. Fig. 1(e) shows the EDX spectrum of the SFO/NZFO composite ferrite nanofibers with mass ratio of 8:2 calcined at 900 °C. The EDX results indicate that the atomic percentage (at%) of Ni, Zn, Sr, Fe and O in the $SrFe_{12}O_{19}/Ni_{0.5}Zn_{0.5}Fe_2O_4$ composite ferrite nanofibers is basically consistent with the designed composition.

Fig. 2 shows the TEM image, HRTEM image and electron diffraction pattern of the SFO/NZFO ferrite composite nanofibers with mass of 8:2 calcined at 900 °C. From Fig. 2(a) and (b), the composite nanofibers are built from SFO nanoparticles about 42 nm and NZFO nanoparticles around 18 nm. The HRTEM image of the ferrite composite nanofiber (Fig. 2(c)) shows sets of lattice fringes of (107) plane from SFO ferrite and (224) plane from NZFO ferrite. The electron diffraction pattern clearly exhibits the diffraction peaks from (107) and (406) planes of SFO ferrite and peaks from (022) and (224) planes of NZFO ferrite. These electron microscopic results prove that SFO ferrite and NZFO ferrite having nanoparticles coexist in the composite nanofiber with a uniform phase distribution. From Fig. 2, the SFO ferrite phase and NZFO ferrite phase somewhat alternatively distributed along the nanofiber length direction. Although this method needs to be further improved, it has provided a route to prepare composite nanofibers with a heterostructure.

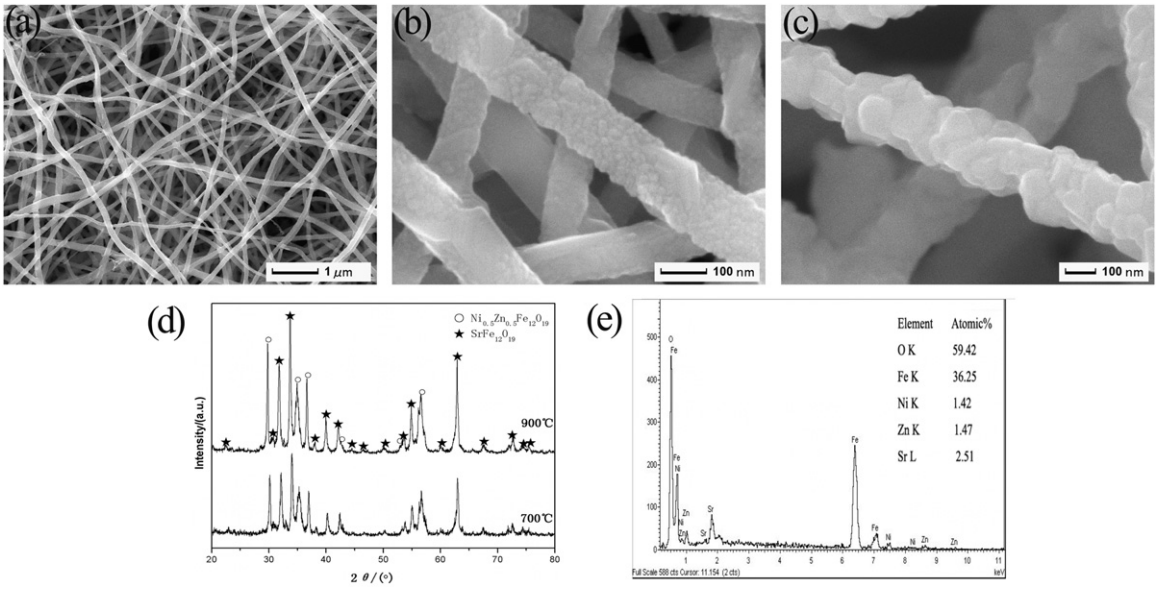

Fig. 1. SEM images (a–c), XRD patterns (d) and EDX spectrum (e) of SFO/NZFO ferrite nanofibers with mass ratio of 8:2 calcined at different temperatures for 2 h.

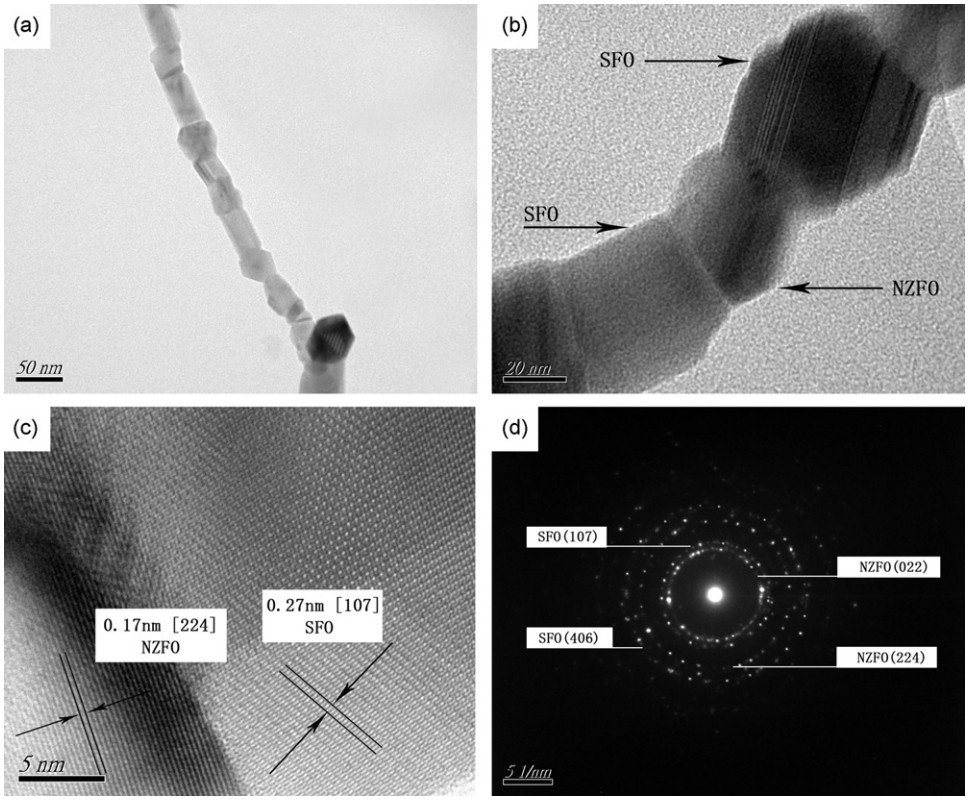

Fig. 2. TEM image (a), HRTEM image (b), (c) and electron diffraction pattern (d) of SFO/NZFO ferrite nanofibers with mass ratio of 8:2 calcined at 900 °C.

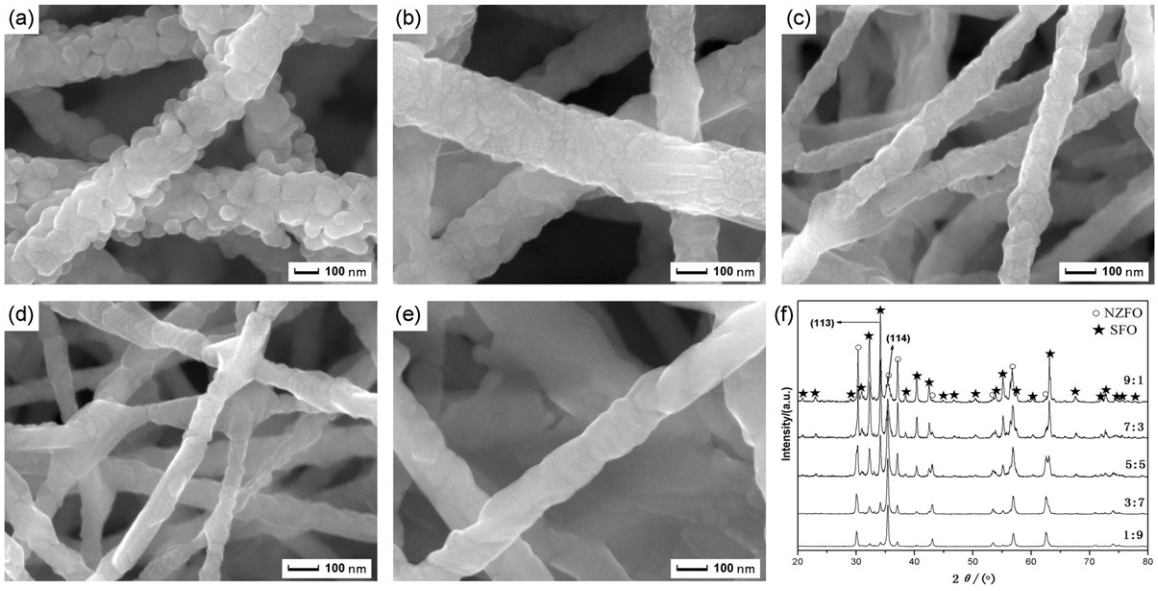

Fig. 3. SEM morphologies and XRD patterns of SFO/NZFO composite ferrite nanofibers with different mass ratios calcined at 900 °C for 2 h: (a) 1:9, (b) 3:7, (c) 5:5, (d) 7:3, (e) 9:1 and (f) XRD patterns with different mass ratios.

Fig. 3 shows SEM morphologies and XRD patterns of SFO/NZFO composite ferrite nanofibers with different mass ratios calcined at 900 °C for 2 h. These nanofibers fabricated of fine nanoparticles possess a uniform diameter around 100 nm and high aspect ratios. With the content of SFO increase, more and more hexagonal plate-like particles emerge on the nanofiber's surface, whilst the particles of NZFO gradually decrease.

Fig. 3(f) shows XRD patterns of SFO/NZFO ferrite nanofibers for different mass ratios calcined at 900 °C for 2 h. From Fig. 3(f) after calcined at 900 °C it shows the coexistence of magnetoplumbite structural SFO phase (JCPDS 33-1340) and spinel NZFO phase (JCPDS 53-0278). However, with content of SFO increase, the reflection peaks corresponding to SFO ferrites become narrower and higher, while the reflection peaks corresponding to NZFO become broader and lower. The average crystallite size (D) of SFO and NZFO ferrites can be calculated from the full-width at half-maximum (FWHM) of the prominent reflection (113) and (114) using Scherrer's equation and the calculated D values are

represented in Table 1. With the mass ratio increasing from 1:9 to 9:1, the crystalline grain sizes of SFO ferrite and NZFO ferrite, as shown in Table 1, are within a nanoscale and increase from 16 to 40 nm (for NZFO ferrite) and decrease from 45 to 19 nm (for SFO ferrite), respectively. This can be explained on the grain growth process due to a higher contact possibility and shorter transfer distances for reactants with the content increase of SFO or NZFO in the composite nanofibers. The SFO ferrite phase inhibits the grain growth of NZFO in the composite nanofibers, which can be ascribed to that the motion of grain boundaries is impeded by the second-phase SFO nanoparticles. As the grain growth through grain boundary migration is usually by a long-range diffusion for a two-phase system with a mutual limited solubility [24], so that, the grain growth will be in some degree controlled by each other owing to the separation effect arising from the presence of the other phase during the calcination process.

The magnetic hysteresis loops of SFO/NZFO composite ferrite nanofibers with different mass ratios calcined at 900 °C for 2 h measured at 297 K are shown in Fig. 4(a) and their magnetic parameters measured at 77 K and 297 K are shown in Table 1.

Table 1
Average crystalline size (D) and magnetic parameters of SFO/NZFO composite ferrite nanofibers with the different mass ratios calcined at 900 °C for 2 h.

Mass ratio (*SFO:NZFO*)	D_{SFO} (nm)	D_{NZFO} (nm)	M_r (A m^2 kg^{-1})		H_c (kA m^{-1})	
			297 K	77 K	297 K	77 K
1:9	40	19	16.1	30.7	7.8	15.2
2:8	33	25	23.2	37.4	19.3	28.1
3:7	31	29	26.3	41.6	39.5	48.6
4:6	28	32	27.1	42.5	73.8	76.6
5:5	26	36	30.1	46.1	121.3	109.8
6:4	23	38	34.2	50.8	223.2	194.8
7:3	21	40	36.3	51.9	296.3	249.8
8:2	18	42	39.1	53.5	379.8	242.2
9:1	16	45	34.8	49.4	356.5	315.5

From Fig. 4a and Table 1, with the mass ratio increasing to 8:2, the coercivity (H_c) and remanence (M_r) initially increase with the grain size from 19 to 42 nm (SFO) and 40 to 18 nm (NZFO), reaching a maximum values of 379.8 kA/m (297 K), 242.2 kA/m (77 K) and 39.1 Am^2/kg (297 K), 53.5 Am^2/kg (77 K), and then show a reduction tendency with a further increase of mass ratio. Compared to the barium ferrite/nickel–zinc ferrite composite powders with the coercivity of 91.2 kA/m (297 K) and remanence of 28.1 Am^2/kg (297 K) reported by Roy and Shivakumara [22], these composite ferrite nanofibers as-prepared in this work have a higher coercivity and remanence (Table 2). This is largely owing to the nanoparticles uniform distribution and coherent interface structures (seen in Fig. 2(a) and (b)).

Generally, the exchange–coupling interaction and dipolar interaction play a major role for the determination of magnetic properties of the composite magnets. According to the three-dimensional model proposed by Han et al. [25] (as shown in Fig. 5), the hard and soft grains are in contact with each other and can be divided into two parts: an inner part without exchange–coupling interaction (uncoupled) and an interfacial part with exchange–coupling interaction (coupled). Therefore, the exchange–coupling interaction only influences the interface layer, which is basically equal to the exchange-length (L_{ex}), and there is no exchange–coupling interaction in the inner part of grains.

As the composite ferrite nanofibers are a mixture of the hard (SFO) and soft (NZFO) phases, there are three types of magnetic interactions. The major one is the interaction between soft–hard grains whereas the other two are the hard–hard and soft–soft [21,26]. Compared to the NZFO ferrite, the SFO ferrite has a high magnetocrystalline anisotropic energy. If there is a sufficient exchange–coupling with the neighboring NZFO ferrite grains, the exchange–coupled interaction will not only align the magnetization in the NZFO ferrite grain but also make the magnetic moments of the interface of the SFO/NZFO composite deviating from the local easy axis and arrange in parallel with each other, which leads to a higher value of magnetization. Since the dipolar

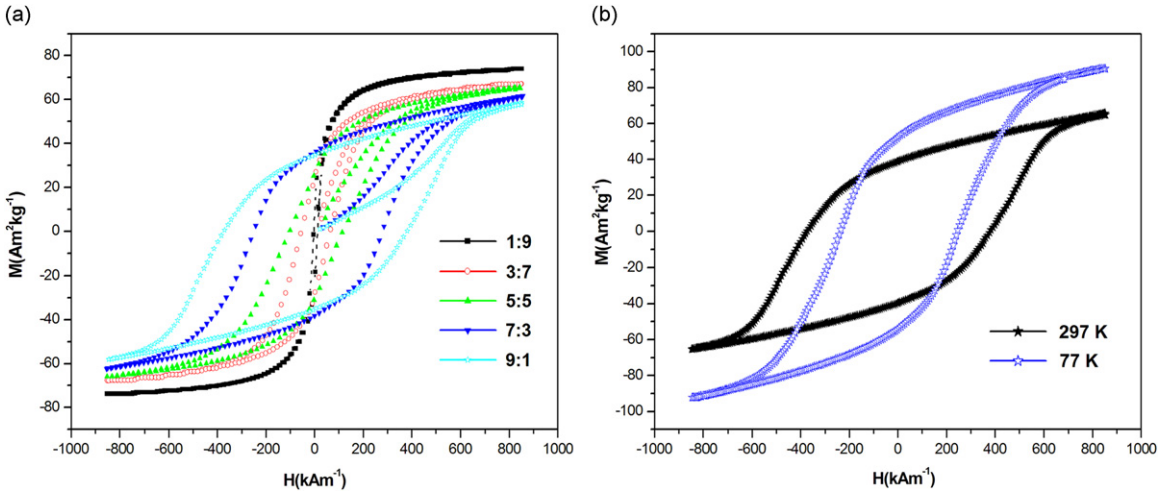

Fig. 4. Magnetic hysteresis loops of SFO/NZFO composite ferrite nanofibers with different mass ratios (a) and with mass ratio of 8:2, measured at 297 K and 77 K (b)

Table 2
Comparison of M_r and H_c for the hard M-type ferrite and the soft spinel ferrite nanocomposite powders and nanofibers with mass ratio of 8:2.

	Preparative routes	M_r (A m^2 kg^{-1})	H_c (kA m^{-1})
$BaFe_{12}O_{19}/Ni_{0.8}Zn_{0.2}Fe_2O_4$ powders [22]	Solid state reaction	27	88
$SrFe_{12}O_{19}/Ni_{0.5}Zn_{0.5}Fe_2O_4$ nanofibers (present work)	Electrospinning and calcination	39	379

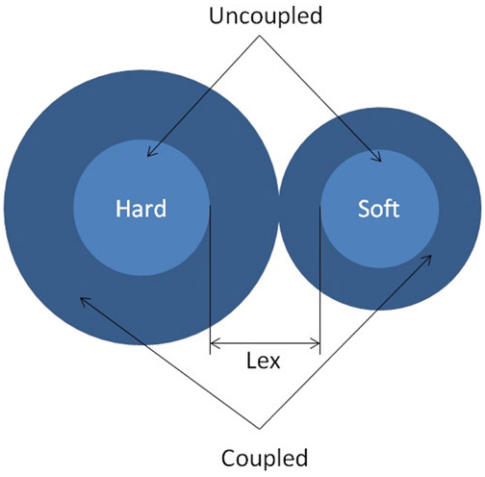

Fig. 5. Illustration of the three-dimensional model of exchange–coupling interactions for hard–soft magnetic grains.

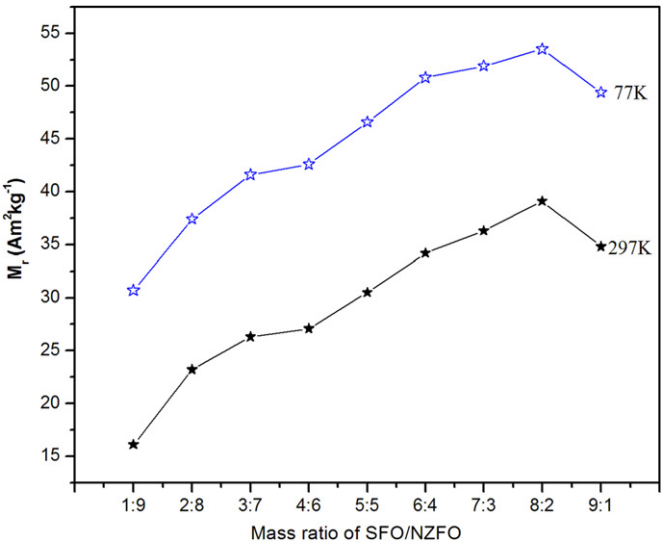

Fig. 6. M_r of composite ferrite nanofibers with the different mass ratios calcined at 900 °C for 2 h, measured at 77 K and 297 K.

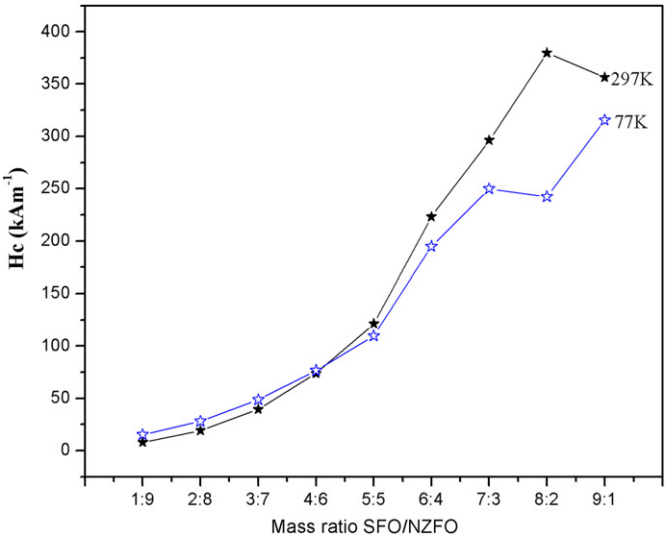

Fig. 7. H_c of composite ferrite nanofibers with the different mass ratios calcined at 900 °C for 2 h, measured at 77 K and 297 K.

interaction is of a long range phenomenon, it will be suppressed by the exchange–coupling interaction, resulting in an increase in H_c and M_r with the mass ratio up to an optimal value (8:2) [21,22,27]. Then, with further mass ratio increase, although the exchange–coupling interactions between the hard–hard phase grains are enhanced, H_c and M_r values are decreased due to a weak dipolar interaction.

According to the theoretical calculation made by Sun et al. [28], in order to exchange couple effectively, the hard grain size should be larger than around 40 nm and the soft grain size should be less than about 15 nm. In the present work, the grain size of the hard phase (SFO) and soft phase (NZFO) of composite ferrite nanofibers with mass ratio of 8:2 are 42 nm and 18 nm, respectively, which is consistent with the theoretical value obtained by Sun et al. [28]. In addition, the structural compatibility in the SFO/NZFO nanocomposite ferrite fibers as analyzed previously is helpful to realize the strong exchange coupling. Thus, the SFO/NZFO composite ferrite nanofibers with the optimal mass ratio can simultaneously combine the high coercivity of SFO ferrite phase and a high specific saturation magnetization of NZFO ferrite phase, and have an enhancement of the remanence, which is a key characteristic of the exchange–coupling interaction [1,29,30].

Fig. 4(b) shows the magnetic hysteresis loops of SFO/NZFO composite ferrite nanofibers with mass ratio of 8:2 calcined at 900 °C for 2 h measured at 77 K and 297 K. From Fig. 4(b), it can be seen that the H_c value (at 77 K) is lower than that at 297 K, while the value of M_r (at 77 K) is higher than the M_r value at 297 K. In order to evaluate the magnetic property of nanocomposite ferrite measured at different temperatures, the estimated M_r and H_c at 297 K and 77 K for the composite ferrite nanofibers with different mass ratios calcined at 900 °C for 2 h are shown in Figs. 6 and 7, respectively. With the mass ratio increase, as shown in Fig. 6, the value of M_r (measured at 77 K) is higher than M_r (measured at 297 K). However, the coercivity exhibits a different behavior from the remanence. From Fig. 7, the coercivity measured at 77 K corresponding to the mass ratio from 1:9 to 4:6 are larger than the values measured at 297 K, whilst it shows a opposite tendency with the further mass ratio increase.The difference between M_r values measured at 297 K and 77 K is related to the surface spin disorder of the nanocrystalline. The surface spin disorder arising from adatoms and clusters adsorbed on the particle surface of the composite ferrite nanofibers makes it harder to align the spins at the surface. At a sufficiently low temperature, the thermal fluctuation on the rotation of magnetic dipoles is suppressed and the surface spin disorder will become spin order. Then, the inverse numbers of spins will decrease, which leads to the M_r increased at a low temperature [31–34].

Contrary to the remanence, the variance of the coercivity measured at 297 K and 77 K can be attributed to the competition of exchange–coupling interaction and thermal fluctuation on dipolar interaction. At low temperatures, the induced anisotropy can no longer be negligible and effective anisotropy in the nanocrystalline can have contributions from the induced anisotropy other than the random mangnetocrystalline anisotropy and hence the effective anisotropy in nanocrystalline can be defined as [10]

$$\langle K\rangle = \sqrt{\langle K_1\rangle^2 + \sum_i K_{ui}^2} \quad (1)$$

where $\langle K\rangle$ is effective anisotropy, K_1 is the random magnetocrystalline anisotropy and K_u is the induced anisotropy. When the mass ratio increases from 1:9 to 4:6, the long range dipolar interaction is more and more pronounced. So that, for the composite ferrite

nanofibers with a relatively high mass ratio the thermal fluctuation on dipolar interaction will play an important role in determination of the magnetic property. At 77 K, the effective anisotropy increases and the influence of thermal fluctuation on the rotation of magnetic dipoles is much restrained. Therefore, a higher magnetic field strength is required to reverse the magnetization direction of these aligned dipoles, which result in a larger coercivity for the composite nanofibers [34, 35]. After the mass ratio increased up to 5:5, the dipolar interaction is suppressed by exchange–coupling interaction and the exchange–coupling interaction dominates in composite ferrite nanofibers. From Fig. 4, the exchange length L_{ex} is a key factor for the exchange–coupling interaction. The increase of effective anisotropy measured at 77 K will result in a decrease in exchange length L_{ex} values according to $L_{ex}=(A/\langle K\rangle)^{1/2}$ and the exchange coupling interaction deteriorates, which lead to the reduction of the coercivity. Therefore, the value of H_c (measured at 77 K) is lower than H_c (measured at 297 K) with the mass ratio from 5:5 to 9:1 and the difference of coercivity measured at 77 K and 297 K has achieved the maximum value at mass ratio of 9:1, which indicate hard and soft grains could be sufficiently exchange–coupled.

4. Conclusions

The magnetic hard/soft $SrFe_{12}O_{19}$ (SFO)/$Ni_{0.5}Zn_{0.5}Fe_2O_4$ (NZFO) composite ferrite nanofibers with different mass ratios and high aspect ratios have been successfully prepared by the electrospinning and calcination process. After calcined at 700 °C for 2 h, the SFO/NZFO composite ferrites have been formed. The composite ferrite nanofibers obtained at 900 °C for 2 h are characterized with diameters ranging from 100 to 150 nm and possess an uniform phase distribution. With the mass ratio of SFO/NZFO increasing from 1:9 to 9:1, the calculated SFO grain sizes increase from about 19 to 45 nm and consequently the NZFO grain sizes reduce from about 40 to 16 nm. Thus the grain size can be controlled by manipulation of the phase institution and calcination process. The mass ratio, particle size and phase distribution are most important factors influencing the magnetic properties of the SFO/NZFO composite ferrite nanofibers. With the hard phase SFO content increasing in the composite, the exchange–coupling interaction is improved whilst the long-range dipolar interaction will be simultaneously suppressed. So that, the SFO/NZFO composite ferrite nanofibers with mass ratio of 8:2 calcined at 900 °C for 2 h exhibit the optimized magnetic properties, with coercivity (H_c) of 379.8 kA/m (297 K), 242.2 kA/m (77 K) and remanence 39.1 Am^2/kg (297 K), 53.5 Am^2/kg (77 K), owing to the enhancement of exchange–coupling interaction resulting from the uniform phase distribution, nanosized grain size and coherent interface structure in the composite ferrite nanofibers. The magnetic difference measured at 297 K and 77 K can be attributed to the surface spin order and exchange–coupling interaction abatement in the nanocomposite ferrite.

Acknowledgments

This work was supported by the National Natural Science Foundation of China (Grant no. 50674048), Research Fund for the Doctoral Program of Higher Education of China (Grant no. 20103227110006) and the Jiangsu Province's Postgraduate Cultivation and Innovation Project (Grant no. CX10B-257Z).

References

[1] L.W. Yin, Y. Bando, Y.C. Zhu, M.S. Li, C.C. Tang, D. Golbera, Adv. Mater. 17 (2005) 213–217.
[2] S. Komarneri, J. Chem. Mater. 2 (1992) 1219–1230.
[3] Y. Choi, J.S. Jiang, J.E. Pearson, S.D. Bader, J.J. Kavich, J.W. Freeland, J.P. Liu, Appl. Phys. Lett. 91 (2007) 072509.
[4] M. Ghidini, G. Asti, R. Pellicelli, C. Pernechele, M. Solzi, J. Magn. Magn. Mater. 316 (2007) 159–165.
[5] T. Tanaka, J. Matsuzaki, H. Kurisu, S. Yamamoto, J. Magn. Magn. Mater. 320 (2008) 2931–2934.
[6] P.S. Doyle, J. Bibette, A. Bancaud, J. Viovy, Science 295 (2002) 2237.
[7] E.F. Kneller, R. Hawig, IEEE Trans. Magn. 27 (1991) 3588–3560.
[8] D. Roy, P.S. Anil Kumar, J. Appl. Phys. 106 (2009) 073902.
[9] J.E. Davies, O. Hellwiga, E.E. Fullerton, Appl. Phys. Lett. 86 (2005) 262503.
[10] K. Suzuki, J.M. Cadogan, Phys. Rev. B 58 (1998) 2730–2739.
[11] K.H. Wu, Y.C. Chang, G.P. Wang, J. Magn. Magn. Mater. 269 (2004) 150–155.
[12] D.A. Allwood, G. Xiong, M.D. Cooke, C.C. Faulkner, D. Atkinson, N. Vernier, R.P. Cowburn, Science 296 (2002) 2003–2006.
[13] F.X. Redl, K.S. Cho, C.B. Murray, S. O'Brien, Nature 423 (2003) 968–971.
[14] Z.L. Wang, X.J. Liu, M.F. Lv, P. Chai, Y. Liu, X.F. Zhou, J. Meng, J. Phys. Chem. C 112 (2008) 15171–15175.
[15] S.O. Hwang, C.H. Kim, Y. Myung, S. Park, J. Park, J. Kim, C. Han, J. Phys. Chem. C 112 (2008) 13911–13916.
[16] H.W. Kwon, I.C. Jeong, A.S. Kim, D.H. Kim, S. Namkung, T.S. Jang, D.H. Lee, J. Magn. Magn. Mater. 304 (2006) e219–e221.
[17] J.P. Liu, Y. Liu, R. Skomski, D.J. Sellmyer, J. Appl. Phys. 85 (1999) 4812–4814.
[18] Soon-Gil Kim, W.N. Wang, T. Iwaki, A. Yabuki, K. Okuyama, J. Phys. Chem. C 111 (2007) 10175–10180.
[19] K.V.P.M. Shafi, I. Felner, Y. Mastai, A. Gedanken, J. Phys. Chem. B 103 (1999) 3358–3360.
[20] P. Xu, X.J. Han, M.J. Wang, J. Phys. Chem. C 111 (2007) 5866–5870.
[21] S. Kohli, P.R. Mcurdy, D.C. Johnson, J. Das, A.L. Prieto, C.D. Rithner, E.R. Fisher, J. Phys. Chem. C 114 (2010) 19557–19561.
[22] Debangsu Roy, C. Shivakumara, P.S. Anil Kumar, J. Magn. Magn. Mater. 321 (2009) L11–L14.
[23] F.Z. Song, X.Q. Shen, M.Q. Liu, J. Xiang, J. Colloid Interf. Sci. 354 (2010) 413–416.
[24] D.N. Fan, L.Q. Chen, Acta Mater. 45 (1997) 4145–4154.
[25] G.B. Han, R.W. Gao, S. Fu, W.C. Feng, H.Q. Liu, W. Chen, W. Li, Y.Q. Guo, Appl. Phys. A 81 (2005) 579–582.
[26] R.W. Gao, W.C. Feng, H.Q. Liu, B. Wang, W. Chen, G.B. Han, J. Appl. Phys. 94 (2003) 664–668.
[27] F. Cabral, F. Machado, J. Araujo, J. Soares, A.R. Rodrigues, A. Araujo, IEEE T. Magn. 44 (2008) 4235–4238.
[28] Y. Sun, R.W. Gao, B.P. Han, M. Liu, G.B. Han, W.C. Feng, Prog. Nat. Sci. 17 (2007) 131–137.
[29] R. Skomski, J.M.D. Coey, Phys. Rev. B. 48 (1993) 15812–15816.
[30] S.D. Yoon, S.A. Oliver, C. Vittoria, J. Appl. Phys. 91 (2002) 7379–7381.
[31] Y.M. Zhao, C.W. Dunnill, Y.Q. Zhu, D.H. Gregory, W. Kockenberger, Y.H. Li, W.B. Hu, I. Ahamad, D.G. McCartney, Chem. Mater. 19 (2007) 916–921.
[32] I. Skorvanek, R. Grossinger, J. Magn. Magn. Mater. 226–230 (2001) 1473–1475.
[33] K. Parekh, R.V. Upadhyay, L. Belova, K.V. Rao, Nanotechnology 17 (2006) 5970–5975.
[34] J. Xiang, X.Q. Shen, F.Z. Song, M.Q. Liu, J. Solid State Chem. 183 (2010) 1239–1244.
[35] D. Li, T. Herricks, Y.N. Xia, Appl. Phys. Lett. 83 (2003) 4586–4588.